PERGAMON

International Journal of Impact Engineering 25 (2001) 553–572

INTERNATIONAL JOURNAL OF IMPACT ENGINEERING

www.elsevier.com/locate/ijimpeng

# Observations on shear plug formation in Weldox 460 E steel plates impacted by blunt-nosed projectiles

Tore Børvik[a,*], John Rasmus Leinum[b], Jan Ketil Solberg[b], Odd Sture Hopperstad[a], Magnus Langseth[a]

[a]*Structural Impact Laboratory (SIMLab), Department of Structural Engineering, Norwegian University of Science and Technology, N-7491 Trondheim, Norway*

[b]*Department of Materials Technology and Electro Chemistry, Norwegian University of Science and Technology, N-7491 Trondheim, Norway*

Received 20 July 2000; received in revised form 10 November 2000; accepted 11 November 2000

**Abstract**

Shear plug formation in circular Weldox 460 E steel plates impacted by blunt-nosed cylindrical projectiles with striking velocities between 100 and 500 m/s has been investigated. Target thickness and projectile impact velocity were the primary variables, and for each target thickness the ballistic limit curve of the material was precisely determined. The test at an impact velocity just below the ballistic limit for each target thickness was selected for a microscopic examination of shear localisation and fracture. In these tests, the plug was pushed only partway through the target, and the localised shear zones outlining the fracture were easily recognised both in the optical and scanning electron microscope. Clear evidence of adiabatic shear bands and material damage due to void growth was found in several of the target plates. Analytical models available in the literature were compared with the results from the experimental and microscopic studies. Reasonable agreement was found between calculations and experiments. 

*Keywords:* Ballistic penetration; Microscopic examination; Shear localisation; Fracture; Analytical models

## 1. Introduction

Structural impact problems have become increasingly important for the industry. In design of offshore structures, account is taken for accidental loads such as dropped objects, collisions,

* Corresponding author. Tel.: + 47-73-59-46-47; fax: + 47-73-59-47-01.
*E-mail address:* tore.borvik@bygg.ntnu.no (T. Børvik).

0734-743X/01/$ - see front matter 
PII: S0734-743X(00)00069-5

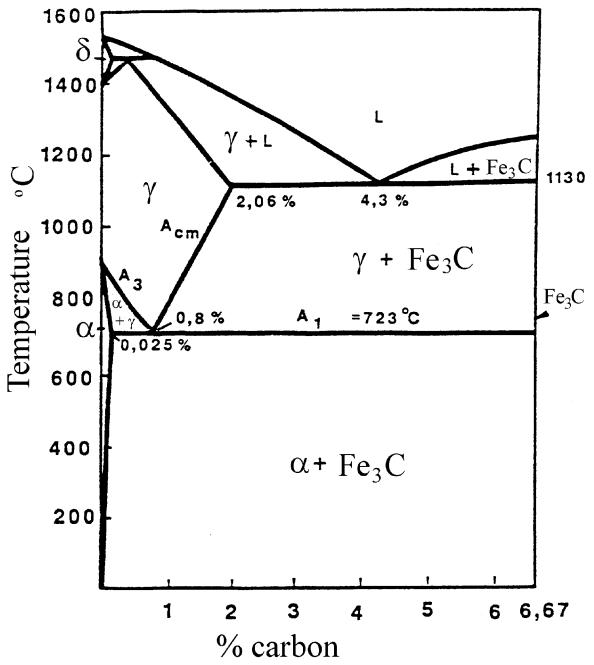


Fig. 1. Part of the Fe–C phase diagram, illustrating the polymorph transformation in Weldox 460 E steel [1].

explosions and fragment penetration. Some of these accidental loads are also pertinent in design of protective structures in the process industry or fortification installations for defence purposes. One typical problem is plugging of plates impacted by blunt-nosed projectiles at moderately high velocities. For relatively thin plates, a combination of localised shearing, bending and membrane stretching absorbs the kinetic energy of the projectile. However, as the plate thickness or projectile velocity is increased, more and more of the kinetic energy is absorbed in local shear zones along the sharp edges of the impacting projectile. Shear bands usually appear when favourable conditions for localised plastic deformation under high strain rate loading exist. A major part of the plastic work conducted during deformation is converted into heat. When the deformation occurs so rapidly that the heat conduction with the surroundings is constrained, the process becomes adiabatic. If the incremental thermal softening overcomes the incremental strain and strain rate hardening, the deformation will localise in narrow zones of intense shear. Within these shear zones the deformation continues under very high local strain rates and temperatures.

In this paper, only the low alloy steel Weldox 460 E is considered. Low alloy steels are polymorph, i.e. they can exist as three different solid phases with different lattice structure depending on the temperature. The three phases are the cubic body centred $\delta$-ferrite, the cubic body centred $\alpha$-ferrite and the cubic face centred $\gamma$-austenite as shown in the Fe–C phase diagram in Fig. 1 [1]. For the investigated Weldox 460 E material, the transformation from $\alpha$ to $\gamma$ starts at 723°C and is completed at approximately 850°C. The latter is the minimum temperature required to form a completely transformed shear band in a penetrated plate. If these temperatures are not reached, there will be no phase change, and the adiabatic shear band should be referred to as

deformed [2]. The microstructure of the transformed bands is determined by the cooling rate from the austenite temperature and by the size of the austenite grains, that in turn is dependent on the maximum temperature and the time for grain growth. With increasing cooling rate, the microstructure will be ferritic/pearlitic, bainitic or martensitic. The latter is a microstructure with carbon in supersaturated solid solution, which makes its crystal structure slightly tetragonal instead of cubic. The hardness of the microstructures increases with increasing cooling rate and decreasing grain size. Transformed adiabatic shear bands are assumed to consist of a martensitic microstructure [2].

Another important softening mechanism is material degradation or damage due to the nucleation, growth and coalescence of microcracks and microvoids. In dynamic problems, this is assumed to occur independently at various material points in the bulk material caused by the short time duration of the transient stress waves. However, material damage is likely to occur inside the adiabatic shear bands where the deformations are extreme and at some point the combination of very large strains and thermal and damage softening leads to failure. The deformation and fracture processes during structural impact have been widely studied over the years, and a comprehensive review on the subject can be found in [3].

Ballistic impact data from tests on 6–30 mm thick steel plates of Weldox 460 E using 20 mm diameter hardened steel rod projectiles with a constant mass of 0.197 kg was recently given by Børvik et al. [4]. In the present study, a microscopic investigation is carried out to examine the local deformations of impacted plates in an attempt to identify and characterise deformed and transformed adiabatic shear bands and to detect material damage in the form of microvoids and microcracks. The test at an impact velocity just below the ballistic limit for each target thickness was selected for a microscopic examination of shear localisation and fracture. In these tests, the plug was pushed only partway through the target, and the localised shear zone outlining the fracture was easily recognised both in the optical and scanning electron microscope. Also some tests where complete perforation occurred were investigated for comparison.

Bai and Johnson [5] presented a model for plugging based on thermoplastic shear instability. The model is valid for plates in which the energy absorption is dominated by shear deformations, i.e. the part of the kinetic energy absorbed in global deformations is assumed to be negligible. Dodd and Bai [6,7] presented approximate equations for the adiabatic shear bandwidth (see also [2] for a comprehensive review on the occurrence and effect of adiabatic shear bands). Data from the impact tests and results from the microscopic investigation are finally discussed in view of these analytical models.

## 2. Experimental set-up and results

The compressed gas gun shown in Fig. 2 was used to launch the sabot-mounted blunt-nosed cylindrical projectiles at impact velocities just below and well above the ballistic limit of the target material. Nominal hardness (HRC 53), diameter (20 mm), length (80 mm) and mass (0.197 kg) of the hardened Arne tool-steel projectiles were kept constant in all tests. The projectile impacted the target plate of Weldox 460 E steel after about 2 m of free flight. The targets were clamped in a circular frame, having a thickness range from 6 to 30 mm and a constant free span diameter of 500 mm. Thus, the only variables in the tests were the target thickness and the initial projectile velocity. If perforation occurred, the projectile and plug were soft recovered in a rag-box. Initial

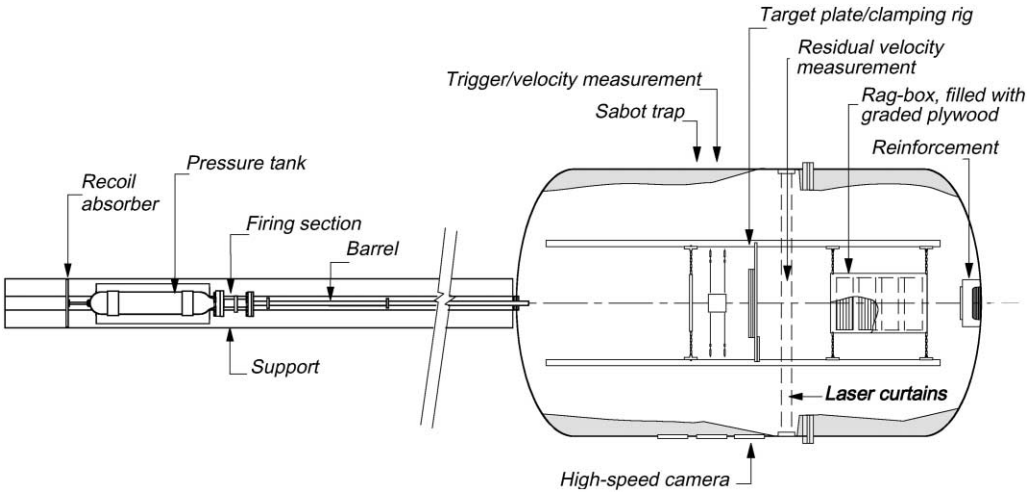


Fig. 2. Sketch of compressed gas gun used in the experiments [9].

Table 1
Estimated ballistic limit velocities ($v_{bl}$) and highest impact velocities ($v_h$) not giving complete perforation [4]. The latter tests were used in the microscopic examinations

| | Target thickness (mm) | | | | | | |
|---|---|---|---|---|---|---|---|
| | 6 | 8 | 10 | 12 | 16 | 20 | 25–30 |
| $v_{bl}$ (m/s) | 145.5 | 154.3 | 165.3 | 184.5 | 236.9 | 293.9 | —[a] |
| $v_h$ (m/s) | 145.3 | 152.5 | 161.2 | 181.5 | 234.3 | 292.5 | 450.2 |

[a] Perforation was not obtained in any of these tests due to projectile shattering at impact.

and final velocities were obtained by different optical measurement systems, and the ballistic limit curve for each target thickness was constructed based on the measured velocities. A digital high-speed camera system was used to photograph the penetration event. Based on the digital images, impact angles and projectile velocity as a function of penetration time were determined. Target oblique and point of impact were also measured. It is referred to [8] for details regarding the experimental set-up and the different measurement techniques used during testing. Projectile and target material data obtained from material tests is presented in [9].

In order to investigate the microstructural details associated with the shear localisation and fracture process, the tests at an impact velocity just below the ballistic limit of each target thickness tested were studied. The ballistic limit for the target is defined as the average of the highest projectile velocity giving only partial penetration and the lowest projectile velocity giving complete perforation [11]. The estimated ballistic limit ($v_{bl}$) for each target thickness is given in Table 1 together with the highest velocity ($v_h$) only giving partial penetration [4]. The difference between $v_{bl}$ and $v_h$ is as seen very small, indicating a precisely determined ballistic limit. Therefore, the tests selected for the microscopic examination were all close to fracture. Fig. 3 shows the ballistic limit

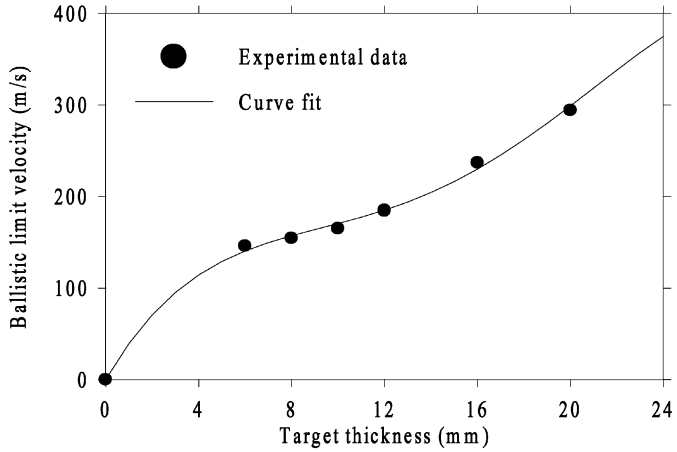


Fig. 3. Ballistic limit velocity versus target thickness [4].

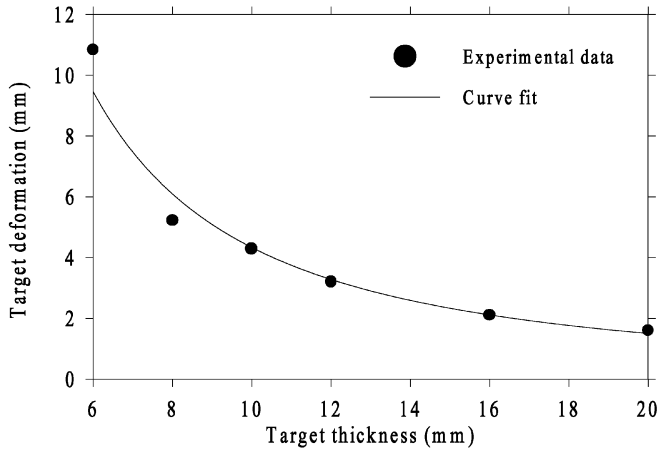


Fig. 4. Target maximum deformation versus target thickness [4].

velocity as a function of target thickness [4]. A distinct kink in the fitted response curve occurs at a target thickness of about 10 mm. This transition in target response appears to be related to a change in deformation mode, from typical thin plate membrane stretching and bending to thick plate shear localisation. The maximum permanent target deformation is given in Fig. 4 [4]. While the in situ measured global deformation is almost twice the target thickness for the 6 mm thick target, it is hardly measurable for 16 and 20 mm thick targets. In thin plates both local and global structural deformations take place. It is here assumed that the global deformation mode absorbs a considerable amount of the projectile kinetic energy during impact. In thick plates, on the other hand, only limited global target deformation can be measured. Hence, most of the kinetic energy has to be absorbed in the highly localised shear zones surrounding the projectile nose. The global

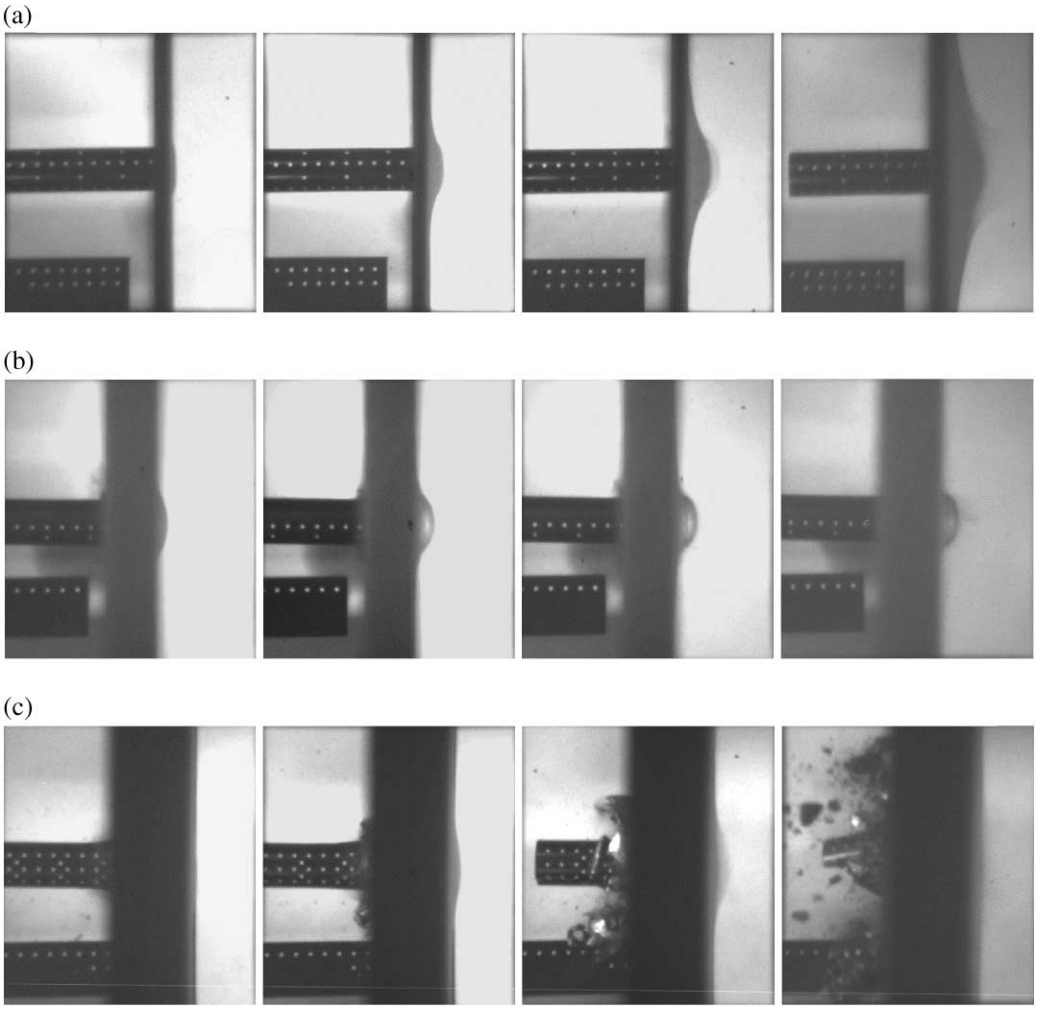


Fig. 5. High-speed camera images from some of the experiments showing penetration of the target without perforation: (a) 6 mm thick target impacted at 145.3 m/s (no perforation); (b) 20 mm thick target impacted at 292.5 m/s (no perforation); (c) 30 mm thick target impacted at 450.2 m/s (no perforation — projectile fracture).

target deformation is also a function of the impact velocity, which reaches a maximum at the ballistic limit velocity independent of target thickness. After perforation, the global target deformation for a given thickness decreases with increasing velocity until it stabilises at a velocity well above the ballistic limit [9].

The high-speed camera images in Fig. 5, showing details from some of the tests, support the above assumptions. As shown in Fig. 5a, the global target deformation in a 6 mm thick target is considerable when the projectile impact velocity is just below the ballistic limit. The actual (i.e. both elastic and plastic) deformation during impact is approximately twice as large as the measured permanent deformation given in Fig. 4. However, this behaviour changes rapidly with target thickness and projectile impact velocity, and for plates in the medium thickness range the

deformation becomes more and more localised even if the projectile velocity is close to the ballistic limit. When the target is thick, the deformation becomes extremely localised. This is clearly seen in Fig. 5b, where the projectile penetrates a 20 mm thick target. Owing to an unsymmetrical failure mode, the projectile may rotate somewhat in the cavity during penetration. For the thickest plates, the projectile is defeated. Fig. 5c shows that a 30 mm thick target shatters the relatively brittle projectile during impact with hardly any visible deformation of the plate. It was not possible to perforate any of the 25 and 30 mm thick targets with the type of projectile used in this study. The projectile also shattered for the highest impact velocities in the tests with 20 mm thick targets. It follows that both impact velocity and target thickness affect the projectile deformation. Projectile shatter was not observed in any of the tests using a target thickness less than 20 mm. It was also found that the projectile indented the front side of the target before any significant deformation could be seen on the rear side. This indentation seemed to increase with target thickness.

## 3. Microscopic observations

Based on the experimental observations, it is seen that both the shear localisation and fracture processes during structural impact are highly affected by target thickness and projectile velocity. As the target thickness and/or projectile velocity are/is increased, the deformation process becomes more and more localised, and for thick targets the deformation mainly takes place in narrow shear zones under extreme strains, strain rates and temperatures. It seems reasonable that such structural behaviour facilitates fracture. Also, at some point the capacity of the hardened projectile may be exceeded and shatter occurs. To verify these observations, and to reveal the physical phenomena underlying the structural behaviour, a microscopic examination of the impacted targets was

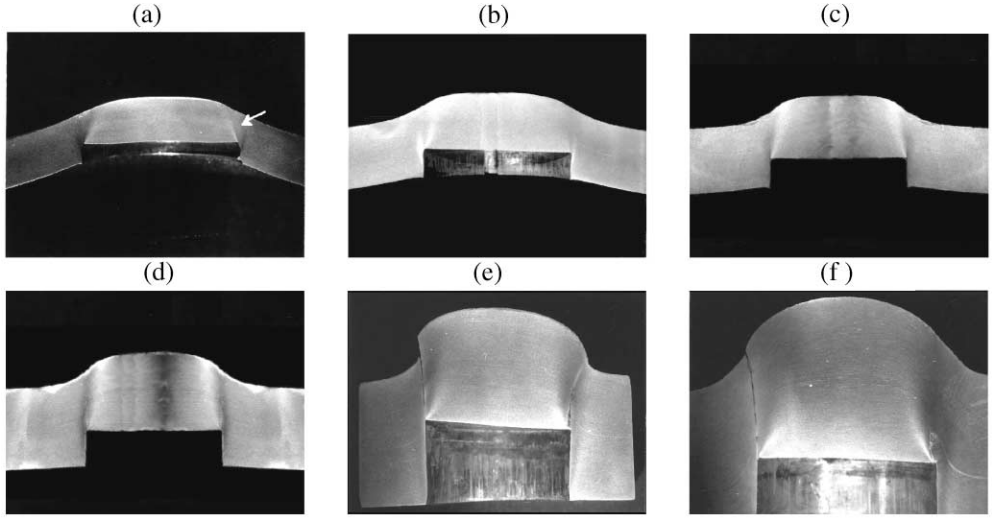


Fig. 6. Macrographs of the cross-section of (a) 6, (b) 8, (c) 10, (d) 12, (e) 16 and (f) 20 mm thick plates penetrated by projectiles with impact velocities just below the ballistic limit. The arrow in (a) indicates the zone where cracking has started.

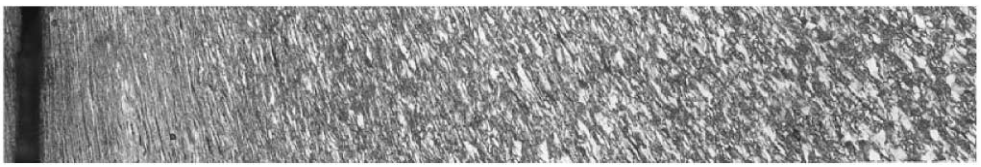

Fig. 7. Micrography of the 10 mm thick plate that shows the change in microstructure towards the shear zone. The crack inside the shear zone can be seen to the left.

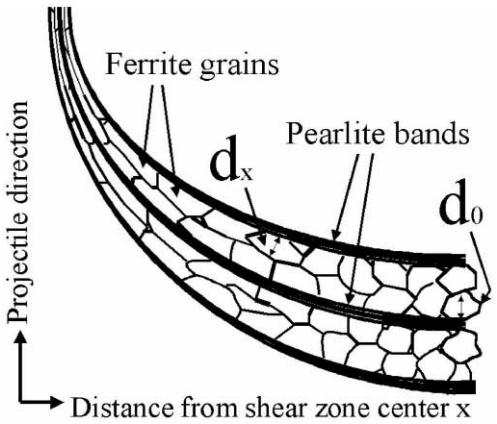


Fig. 8. Sketch of the ferritic/pearlitic microstructure used in the measurements of the local deformation, showing ferrite grains between pearlite bands analogue to Fig. 7. For simplicity, the pearlite bands are drawn as continuous bands.

accomplished. It is also known that both the mechanical and thermal properties of the target material itself are important regarding the presence or absence of adiabatic shear bands during structural impact [2], but the effect of varying material properties has not been investigated in this study.

The studies of the cross-sections of penetrated plates were carried out in a Leica MeF4 light microscope equipped with a ProgRes 3008 digital video camera and in a Jeol JSM 840 scanning electron microscope. Hardness measurements were carried out in a Matsuzawa MXT70 digital micro-hardness tester with a Vickers pyramid, applying a load of 50 g for 15 s. Most plates studied were impacted at velocities just below the ballistic limit. The macroscopic images in Fig. 6 clearly illustrate that the intensity of the deformation in the localised shear zone increases with plate thickness. The change in microstructure along the mid-thickness plane of a 10 mm thick plate towards the shear zone is given in Fig. 7. In the centre of the shear zone a strong plastic deformation has taken place, leading to a reduction of the distance between the pearlite bands in the material and consequently a reduced grain diameter. At a position $x$, a measure of the local dimensionless deformation $\varepsilon_x$ of the ferrite grains is defined as (Fig. 8)

$$\varepsilon_x = \ln \frac{d_0}{d_x}, \tag{1}$$

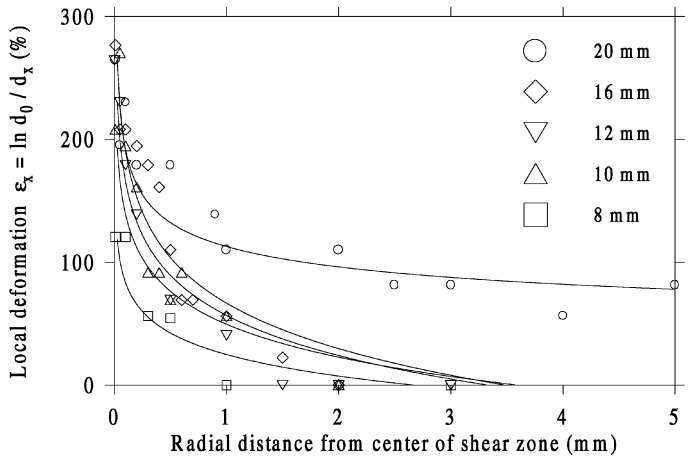


Fig. 9. Microscopic measurable deformation as a function of distance from the shear zone in plates of varying thickness penetrated at impact velocities just below the ballistic limit.

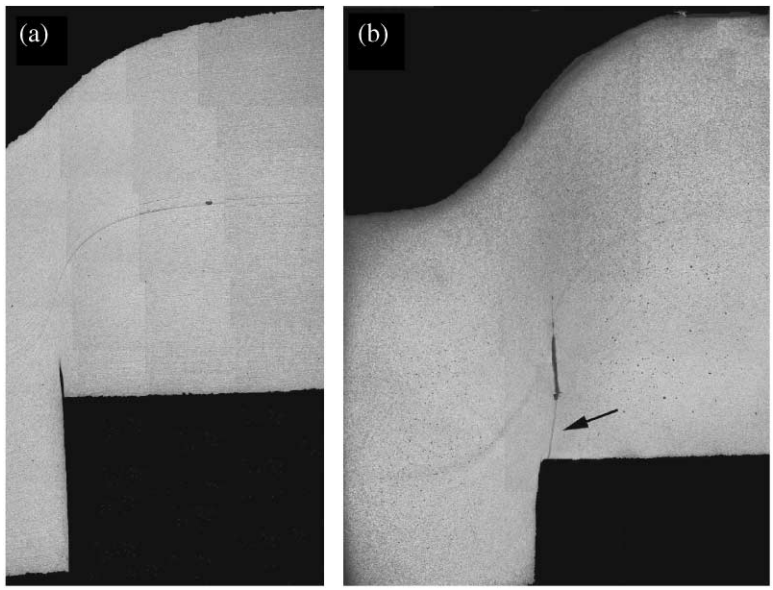


Fig. 10. (a) Micrography of penetrated 16 mm thick plate and (b) micrography of penetrated 20 mm thick plate. The arrow points at a transformed adiabatic shear band in the 20 mm thick plate.

where $d_0$ is the grain diameter as measured normal to the pearlite bands in the undeformed matrix far from the shear zone, and $d_x$ is the value at position $x$. Fig. 9 shows the measured variation in $\varepsilon_x$ as a function of distance from the centre of the shear zone in plates of varying thickness penetrated by projectiles with impact velocities just below the ballistic limit (see Table 1). In the microstructural investigation it was found that the deformation in the pearlite bands far from the middle of the shear zone is too small to be measured. However, the extension of the localised zone with microscopic observable deformation increases with increasing plate thickness, Fig. 9,

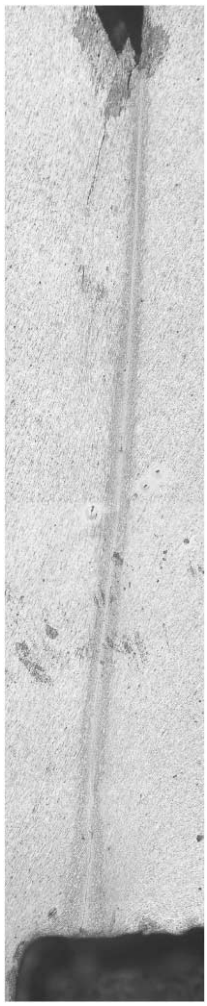

Fig. 11. Transformed adiabatic shear band in the 20 mm thick plate penetrated at an impact velocity just below the ballistic limit.

in contrast to the global target deformation that decreases with increasing plate thickness, Fig. 4.

A large zone of high deformation causes an increased temperature, and transformed shear bands may occur, as in the thickest plates. Fig. 10 gives a comparison of the shear zones in the 16 and 20 mm thick plates, and a transformed adiabatic shear band in the 20 mm plate becomes visible in the lower part of the zone. Fig. 10 also indicates the contour of the sigmoidal shape of the flow lines in the most strained part of the shear zone. The micrographs in Figs. 11 and 12 are magnifications of a transformed adiabatic shear band in the 20 mm thick plate. Close to the projectile entrance a crack has formed within the band. At $1000\times$ magnification, Fig. 12, it is seen that a new microstructure has formed in the band because the $A_3$ temperature has been exceeded (see Fig. 1). At this high magnification, the crack following the centre of the shear band can easily be seen.

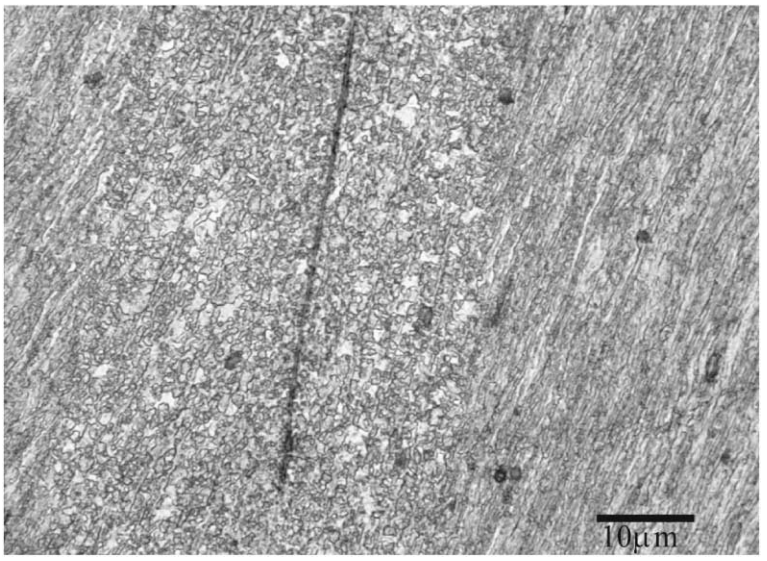


Fig. 12. A 1000× magnification of the adiabatic shear band in the 20 mm thick plate shows a new microstructure as a result of the polymorph phase-transformation in low alloy steels when the temperature crosses the $A_3$ transformation temperature.

Vickers hardness measurements of the cross-sections show a strong increase in hardness in the transformed shear band compared to the surroundings both for the 20 and 25 mm thick plates, Fig. 13. The hardness of the shear band was compared with that obtained in a thin plate of Weldox 460 E steel homogenised at 930°C and quenched in cold water to obtain a martensitic microstructure. This microstructure is shown in Fig. 14, and differs from the microstructure in the adiabatic shear band in Fig. 12 by its coarse grain size. The hardness of this martensite was 420 $HV_{50g}$, approximately equal to the hardness measured in the adiabatic shear band in the 20 mm plate, but 30 $HV_{50g}$ lower than the hardness of the shear band in the 25 mm plate. It is reasonable to conclude that the transformation structure in the shear band is martensite, and that the relatively high hardness values are due to an extremely fine-grained structure. It is further assumed that the grain boundaries visible within the adiabatic shear band in Fig. 12 are previous austenite grain boundaries and that the martensite laths are so fine that they are not resolved in the image. The original hardness of the plates was 180–190 $HV_{50g}$.

A study in the scanning electron microscope (SEM) was done to identify the mechanisms for crack propagation during the penetration process. The cross-section SEM micrographs in Fig. 15 show a crack in the 12 mm thick plate. It is seen that voids are present in front of the crack tip, and that secondary voids have formed in a narrow zone around the crack. Such void growth in front of the crack tip has also been identified in 10 mm thick plates [9]. A special case is the 20 mm thick plate given in Fig. 16a, showing a transformed adiabatic shear band that contains a longitudinal crack. Around this crack is a fully transformed zone where ferrite and pearlite have been transformed into austenite under heating and then into martensite due to the rapid cooling. On both sides of this zone the material is partially transformed and contains both martensite and ferrite. The material has reached the temperature where austenite and ferrite co-exist (Fig. 1), and

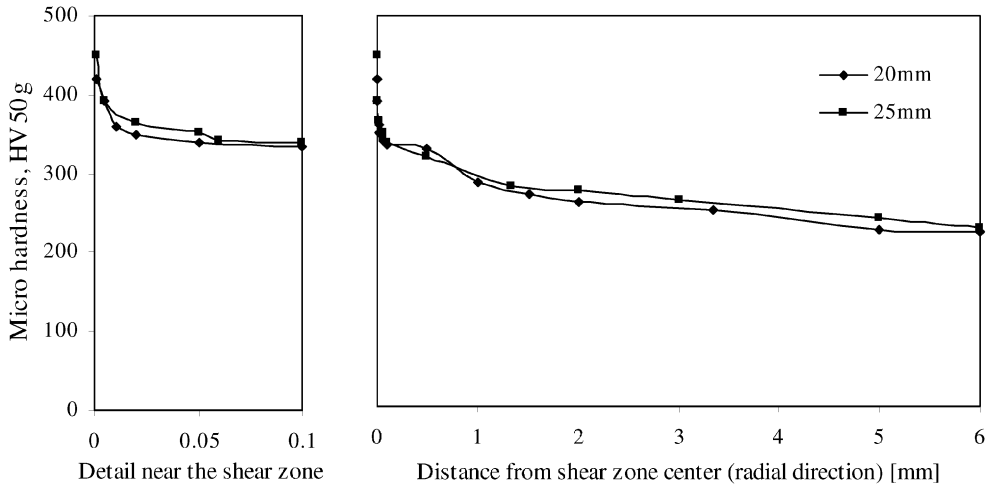


Fig. 13. Vickers hardness measurements of cross-sections show a considerable increase in hardness in the transformed shear-bands that correspond to the martensite hardness of Weldox 460 E steel, $HV_{50g} = 420$.

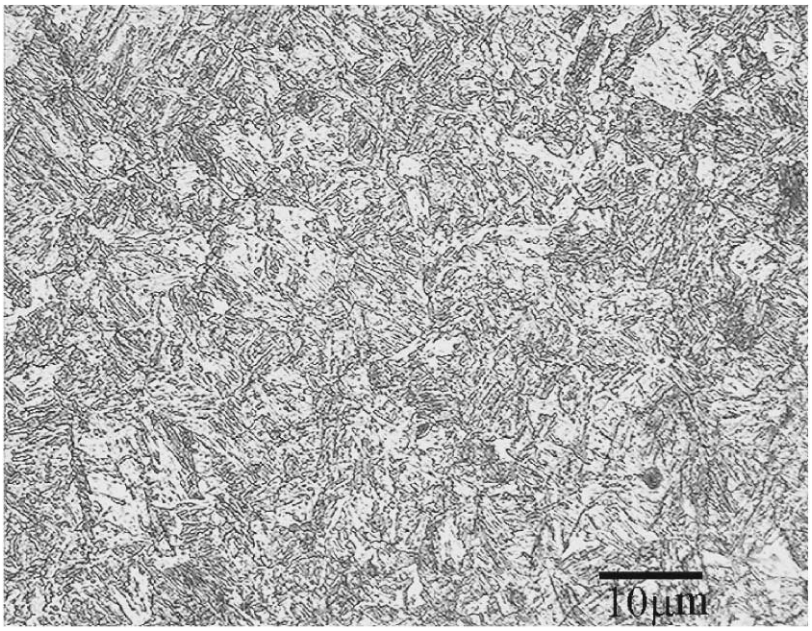


Fig. 14. Martensitic grain structure in a 2 mm thick sample of Weldox 460 E steel heat treated at 930°C and quenched in cold water. The previous austenite grain size is approximately 10 μm.

after rapid cooling austenite has been transformed into martensite. Ferrite has a higher self-diffusivity than austenite and ferrite grain growth in the partially transformed zone can be seen. Secondary microcracks and voids found outside the transformed shear band are shown in Fig. 16b. Probably, this is an example of the simultaneous propagation of two independent cracks. SEM

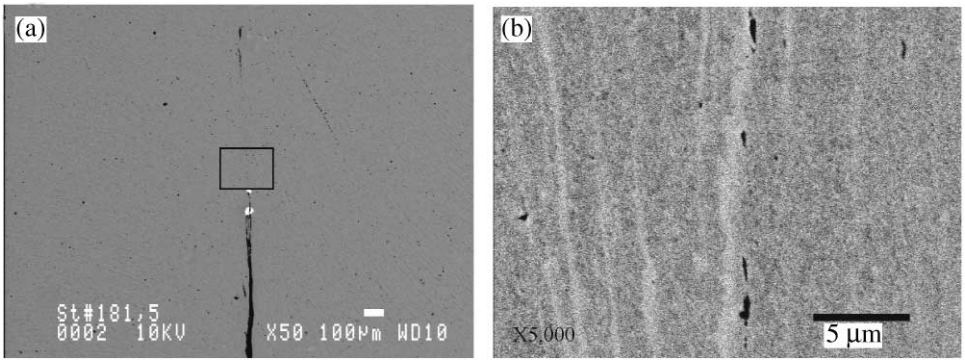


Fig. 15. (a) Scanning electron micrography at 50× magnification shows the cross-section of a 12 mm plate in an area around the crack and the formation of voids in front of the crack-tip with secondary voids in a narrow area around the crack-tip. (b) At 5000× magnification of the frame in (a) small voids in front of the crack-tip in the 12 mm thick plate can be seen.

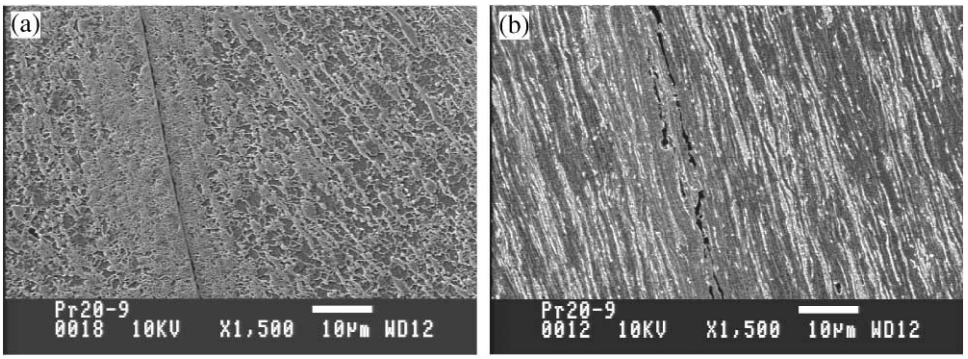


Fig. 16. (a) A crack in the transferred adiabatic shear band and (b) voids and secondary cracks outside the adiabatic shear band in the 20 mm thick plate.

investigations of the fracture surface of a perforated plate confirmed the formation of voids as the main fracture mechanism, Fig. 17b. In this case, the projectile has deformed the initial part of the fracture surface, leaving a smooth surface that resembles the surface of an extruded product, Fig. 17a. Investigations of a statically penetrated 10 mm thick plate showed the same type of fracture surfaces as in the dynamically penetrated 10 mm thick plate.

Finally, Fig. 18 shows a macroscopic image of a fractured projectile within the target after impacting a 25 mm thick plate at an initial velocity of approximately 450 m/s. As seen, after the initial indentation the nose part of the projectile is completely shattered, and the penetration process terminates. Only a limited amount of shear localisation seems to have occurred before projectile breakdown, and no proof of transformed adiabatic shear bands propagating towards the rear side of the target was found. However, a closer examination revealed incipient shear bands inclined to the impact direction, similar to the theoretical slip-line field solution for indentation [2].

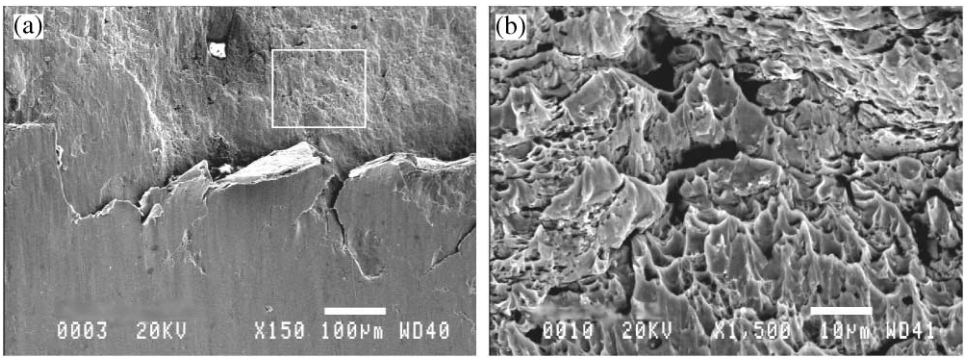


Fig. 17. (a) Scanning electron micrography of the fracture surface of the 10 mm thick plate with both a ductile dimple structure and plane areas deformed by the projectile and (b) details from the frame in (a) of the dimple structure at 1500× magnification.

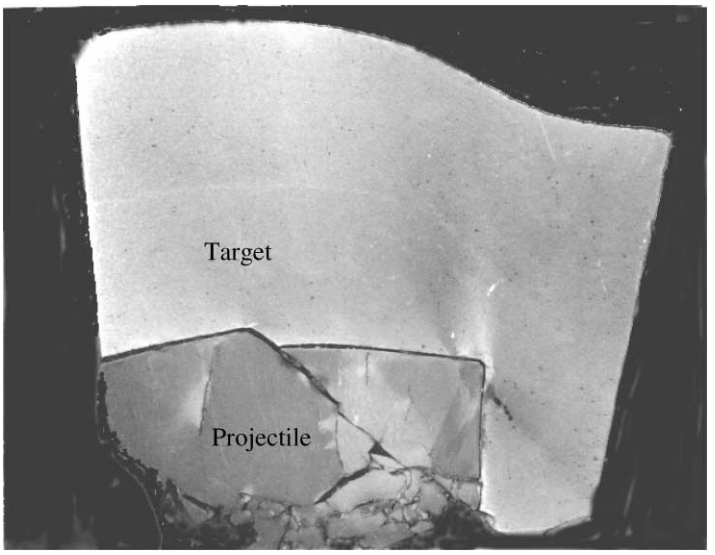


Fig. 18. Fractured projectile in a 25 mm thick target at an impact velocity of 450 m/s.

Shear bands propagating perpendicular to the impact direction can give fragmentation of the target, but no plugging. Woodward et al. [12] reported similar behaviour in the penetration of thick aluminium targets by blunt-nosed projectiles.

## 4. Discussion

An experimental study on the ballistic penetration of circular Weldox 460 E steel plates impacted by blunt-nosed cylindrical projectiles has been carried out. The experimental details from the

component tests are presented in [4], but one major observation quoted here is the distinct kink in the ballistic response curve at a target thickness of about 10 mm (Fig. 3). This transition in target response appears to be related to the change in deformation mode with target thickness, from typically thin plate global deformation to thick plate shear localisation. When the target thickness is sufficiently increased the hardened projectile fractures at impact and shear plugging is prevented (see Fig. 5c). The subsequent metallographic examination of the impacted targets confirmed that for plates of thickness about equal to or larger than the projectile radius (i.e. $b \geqslant 10$ mm, where $b$ is the target thickness), the plugging process was dominated by adiabatic shear deformation in localised bands. For thinner plates, i.e. $b < 10$ mm, the plugging process seemed to be controlled by a combination of localised shear, bending and tension. For plates of thickness between 10 and 16 mm, the adiabatic shear bands were only deformed, which means that no phase transformed material was found in the zones of intense plastic strain. However, clear evidence of transformed adiabatic shear bands causing extreme strains, strain rates and temperatures was found in plates equal to or thicker than 20 mm. In other words, the local plugging process seems to be controlled by at least three distinctly different deformation modes depending on the target thickness.

It is very difficult to quantify parameters such as the shear bandwidth, temperature rise, critical strain and strain rate in the localised zones due to a diffuse and complex microstructure within the deformed area. However, in the deformed adiabatic shear bands the bandwidth seemed to be more than 100 μm (typically 200–300 μm). The intensity of the band was found to increase almost exponentially towards the centre, while the width of the band increased linearly throughout the thickness of the plate and became very diffuse due to the influence of tensile forces at the rear side. No transformed shear bands were found in target plates having a thickness less than 20 mm. This indicates that the phase transformation temperature of 723°C was not reached in any of these tests. The transformed adiabatic shear bands in the thickest plates were easier to identify, but also these bands showed a somewhat diffuse microstructure. The width of the band in the most intense zone was about 10–20 μm. Here, a complete phase transformation took place, indicating a temperature above 850°C. However, the width of the entire shear band was measured to be between 40 and 100 μm. In the outer area, the material was only partially transformed, and the temperature is assumed to have been between 723 and 850°C (see Fig. 1). The width of the transformed band was almost constant throughout its length, while the width was found to increase with increasing target thickness (Fig. 9).

Accordingly, shear instability and localisation play a major role in plugging of steel plates impacted by blunt projectiles. It is therefore of interest to compare the results with available analytical models for plugging based on such behaviour. A large literature exists on the subject concerning the occurrence, formation and evolution of adiabatic shear bands, and much of this work has been gathered in [2]. However, fewer publications have considered the plugging process followed by adiabatic shear banding. Bai and Johnson [5] developed a simple mechanical model for plugging based on adiabatic shear instability. The model consists of three major elements: the kinetic energy equation connecting the projectile and the plug, the constitutive equation, and the relationship between the displacement of the plug and the shear strain. It is assumed that only simple shear deformation occurs in the direction of the projectile when in the plate. A necessary criterion for shear instability is that temperature softening outbalance the strain and strain rate hardening, i.e. that the increment in shear stress is equal to or

less than zero in a loading process

$$\delta\tau = \frac{\partial f}{\partial \gamma}\delta\gamma + \frac{\partial f}{\partial \dot{\gamma}}\delta\dot{\gamma} + \frac{\partial f}{\partial \theta}\delta\theta \leqslant 0, \tag{2}$$

where $\tau = f(\gamma, \dot{\gamma}, \theta)$, i.e. that the shear stress $\tau$ is a function of shear strain $\gamma$, shear strain rate $\dot{\gamma}$ and temperature $\theta$. Bai and Johnson [5] assumed that the effect of strain rate variation is negligible at high strain rates and that the effect of temperature softening caused by adiabatic heating could be implicitly accounted for. Thus, a constitutive relation on the form $\tau = f(\gamma)$ was adopted, and the shear instability criterion from Eq. (2) is simplified to

$$\delta\tau = \frac{\mathrm{d}\tau}{\mathrm{d}\gamma}\delta\gamma \leqslant 0. \tag{3}$$

The particular adiabatic constitutive equation used by Bai and Johnson in their model was expressed in terms of the shear strain as

$$\tau = \tau_{\mathrm{M}}\left(\frac{\gamma}{\gamma_i}\right)^n \exp\left\{\frac{n}{1+n}\left[1 - \left(\frac{\gamma}{\gamma_i}\right)^{n+1}\right]\right\}, \tag{4}$$

where the maximum shear stress, $\tau_{\mathrm{M}}$, and the critical value of the shear strain, $\gamma_i$, at which $\delta\tau = 0$, were found as

$$\tau_{\mathrm{M}} = \tau_0(1 + \alpha\theta_0)\gamma_i^n \exp\left(-\frac{n}{1+n}\right)$$

and

$$\gamma_i = \left(-n\frac{\rho C_v}{\alpha\tau_0}\right)^{1/(1+n)}. \tag{5}$$

Here, $\tau_0$ and $\alpha$ are material constants, $\theta_0$ is the initial temperature, $C_v$ is the specific heat, $\rho$ is the density and $n$ is the strain hardening index of the material. Thus, it is seen that the shear localisation depends on the strength and strain hardening characteristics of the material, the material density and the thermal properties. More details regarding the model and all the essential equations can be found in the original paper by Bai and Johnson [5].

The material properties of Weldox 460 E steel have been identified by Børvik et al. [9,10] through a test programme including tensile tests in different material directions, at high strain rates, at high temperatures and with different levels of hydrostatic tension. The material constants required in Eq. (4) for Weldox 460 E have been determined from the experimental data as $\gamma_i = 1.4$, $\tau_M = 570\,\mathrm{MPa}$ and $n = 0.25$. It is here assumed that the shear stress and shear strain can be calculated based on the von Mises relations as $\tau = \sigma_{\mathrm{eq}}/\sqrt{3}$ and $\gamma = \sqrt{3}\varepsilon_{\mathrm{eq}}$, where $\sigma_{\mathrm{eq}}$ and $\varepsilon_{\mathrm{eq}}$ are the von Mises equivalent stress and strain, respectively. The assumed adiabatic shear stress–strain curve from Eq. (4) is shown in Fig. 19.

Instead of modelling the fracture process, involving nucleation, growth and coalescence of microcracks and voids, Bai and Johnson [5] assumed that the penetration process terminates at a penetration depth $p_{\mathrm{U}} = b$, i.e. at a penetration depth equal to the target thickness. It was argued that for metals considerable amounts of energy can be absorbed in post-instability deformation,

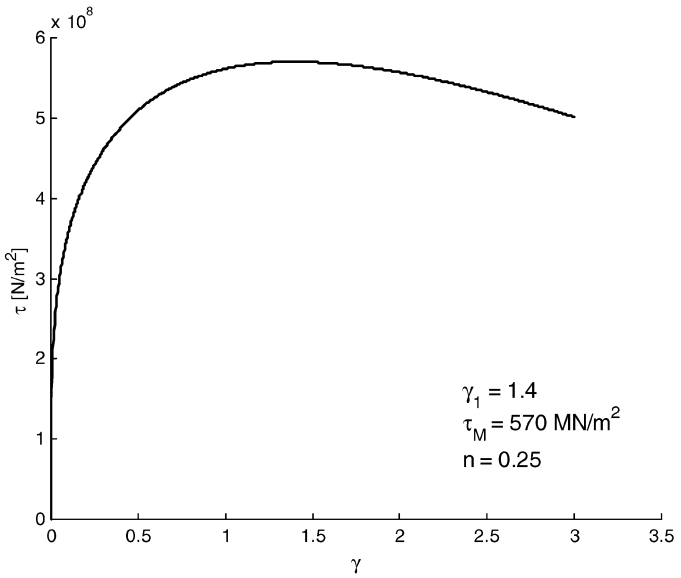


Fig. 19. Adiabatic shear stress–strain curve for Weldox 460 E from the Bai–Johnson model.

and in this sense the assumption is reasonable. The approach is assumed to give an upper limit to the energy absorption in plugging. However, some experimental results indicate that fracture occurs when the projectile is approximately halfway through the target (see e.g. [9]). Thus, the termination of the penetration process can also be defined by $p_U = b/2$.

The ballistic limit velocity $v_{bl} = v_{0C}$ obtained with the Bai–Johnson model for plugging is plotted in Fig. 20a against target thickness $b$ both for $p_U = b$ and $p_U = b/2$. The penetration time $t(p_U)$ and the ultimate temperature $\theta_a(p_U)$ as functions of target thickness for a striking velocity $v_{0C}$ are presented in Figs. 20b and c. The nominal values of density and specific heat for steel are adopted as $\rho = 7850\,\mathrm{kg/m^3}$ and $C_V = 452\,\mathrm{J/kg\,K}$ [9]. It is seen in Fig. 20a that $p_U = b$ overestimates the plugging capacity of the target plates, while $p_U = b/2$ is in good agreement with the experiments for $b \geqslant 12\,\mathrm{mm}$, which corresponds well with the assumed domain of validity for the Bai–Johnson model. For thinner plates the contribution from global deformations is considerable. The perforation time is given in Fig. 20b. The model predicts perforation times between 120 and 140 μs for plates with thickness from 12 to 20 mm when $p_U = b$, while for $p_U = b/2$ the perforation time is constant about 80 μs. These values are reasonably close to the experimentally measured perforation times of about 100 μs independent of target thickness [4]. Based on the microscopic study, it is assumed that the temperature in the adiabatic shear band in the 20 mm thick target plates was slightly above 850°C. The Bai–Johnson model with $p_U = b$ predicts a maximum temperature of about 800°C for the 20 mm thick plate, while for $p_U = b/2$ the temperature is only slightly above 450°C, see Fig. 20c.

In order to estimate the width of the adiabatic shear band, a model that takes into account both heat generation from plastic work and thermal conductivity is needed. Dodd and Bai [6] derived an equation for the half-width $\delta$ of an adiabatic shear band based on Bai's approximate model for

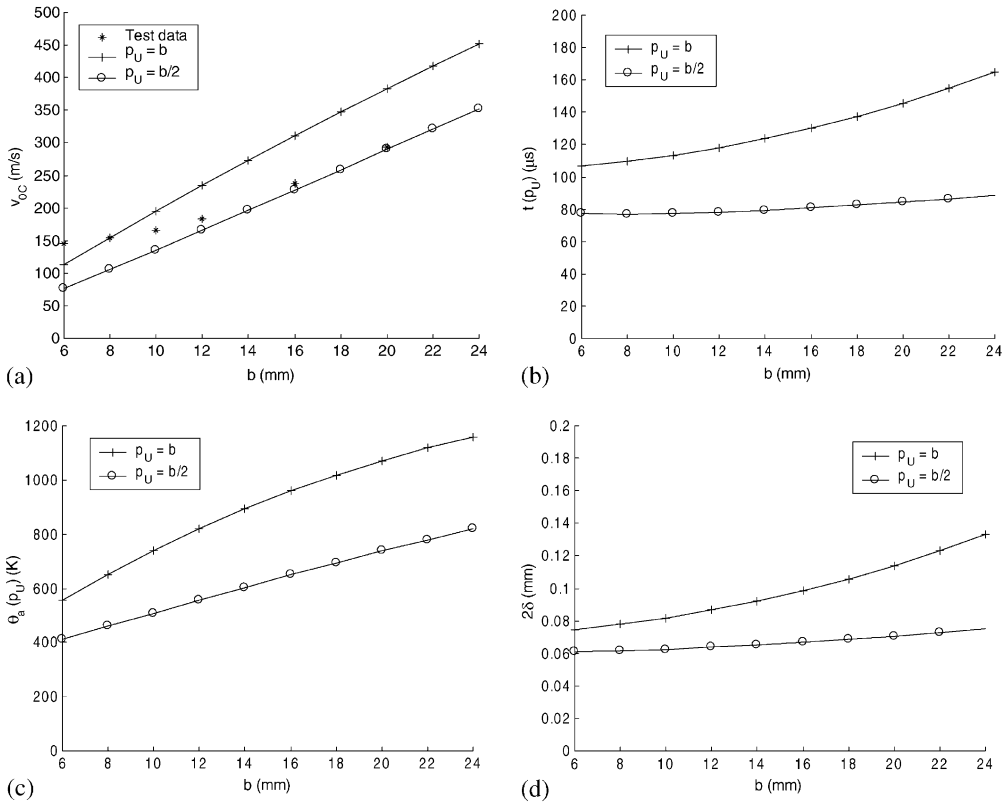


Fig. 20. Results from analytical model of (a–c) Bai and Johnson [5] and (d) Dodd and Bai [6]. The impact velocity in (b)–(d) is equal to the ballistic limit velocity at the actual target thickness.

simple shear [13], while combined stresses were considered in [7]. The equation shows, in accordance with a number of separate experimental observations, that the bandwidth depends on the thermal properties of the material and the rate of dissipated work, but is independent of the details of the combined stress state [7]. For simple shear, the equation for the half-width of the adiabatic shear band reads [6]

$$\delta \approx \left( \frac{\lambda \Delta\theta_*}{K \tau_* \dot{\gamma}_*} \right)^{1/2}, \tag{6}$$

where the subscript $*$ denotes characteristic quantities within the band. The quantities $\tau_*$, $\dot{\gamma}_*$ and $\Delta\theta_* = \theta_* - \theta_0$ are not easily found experimentally, and some approximations have to be adopted. Here the Bai–Johnson model is used to obtain approximations for the quantities within the shear band. $\tau_*$ and $\Delta\theta_*$ are approximated by the predicted values of shear stress and temperature increase at termination of the plugging process, while $\dot{\gamma}_*$ is the average strain rate (i.e. shear strain divided by time at $p = p_U$). $K$ is the fraction of plastic work converted into heat. Here, $K$ is chosen equal to 1 for simplicity. The thermal conductivity for Weldox 460 E steel is taken as $\lambda = 50$ W/m K

[6]. The adiabatic shear bandwidth $2\delta$ is plotted in Fig. 20d against target thickness $b$ for $p_U = b$ and $p_U = b/2$. It is found that $2\delta$ is in the order of 50–100 μm, which is in reasonable agreement with the experimental observations.

## 5. Conclusions

Shear plug formation in Weldox 460 E steel plates impacted by blunt-nosed steel rod projectiles was studied. Plates from impact tests with striking velocity just below the ballistic limit for 6–30 mm thick targets were selected for a microscopic investigation of the shear localisation and fracture. In these tests, the plug was pushed only partway through the target, and the localised shear zones outlining the fracture were easily recognised in the microscope.

Both from post-impact measurements and high-speed camera images of the penetration process it was found that the global deformations decreased rapidly with increasing target thickness, and for targets of 16 mm thickness or more the global deformation was almost negligible. This indicates that the kinetic energy of the impacting object is mainly absorbed as local deformations in narrow shear zones around the periphery of the projectile. The microscopic study showed clear evidence of adiabatic shear bands; deformed shear bands in 10–16 mm thick targets, transformed shear bands in thicker targets. The width of the shear bands ranged from 100 to 300 μm in deformed bands and from 10 to 100 μm in transformed bands. Microcracks and microvoids were found inside the shear bands, and in front of the propagating crack. This indicates a fracture process as follows. The shear deformation is localised in narrow bands because of thermal softening and thermoplastic instability. In the adiabatic shear bands, extreme strains occur, leading to nucleation and growth of microvoids and microcracks. The material damage leads to further softening and an even stronger localisation of the deformation. Fracture occurs when the voids and cracks coalesce into a macrocrack by necking down of the matrix material between them.

The analytical model of Bai and Johnson was used to predict the plugging process, and reasonable results were obtained, taking into account the simplicity of the model. The model proposed by Dodd and Bai predicted the width of the adiabatic shear bands with reasonable accuracy.

## Acknowledgements

The financial support of this study by the Norwegian Defence Construction Service, Central Staff/Technical Division, Oslo, Norway, is gratefully acknowledged.

## References

[1] Solberg JK. Teknologiske Metaller og Legeringer. Department of Material Science and Electro Chemistry, Norwegian University of Science and Technology (NTNU), 1999 [in Norwegian].
[2] Bai Y, Dodd B. Adiabatic shear localization. Occurrence, theories and applications. Oxford: Pergamon Press, 1992.
[3] Zukas JA, editor. High velocity impact dynamics. New York: Wiley, 1990.

[4] Børvik T, Hopperstad OS, Langseth M, Malo KA. Effect of target thickness in blunt projectile penetration of Weldox 460 E steel plates. 2000, submitted for publication.
[5] Bai YL, Johnson W. Plugging: physical understanding and energy absorption. Metals Technol 1982;9:182–90.
[6] Dodd B, Bai Y. Width of adiabatic shear bands. Mater Sci Technol 1985;1:38–40.
[7] Dodd B, Bai Y. Width of adiabatic shear bands formed under combined stresses. Mater Sci Technol 1989;5:557–9.
[8] Børvik T, Holen K, Langseth M, Malo KA. An experimental set-up used in ballistic penetration. Proceedings of Fifth International Symposium on Structures under Shock and Impact, Thessaloniki, Greece, 24–26 June 1998. p. 683–92.
[9] Børvik T, Langseth M, Hopperstad OS, Malo KA. Ballistic penetration of steel plates. Int J Impact Engng 1999;22:855–86.
[10] Børvik T, Hopperstad OS, Berstad T, Langseth M. A computational model of viscoplasticity and ductile damage for impact and penetration. Eur J Mech A/Solids 2001, in press.
[11] Backman ME, Goldsmith W. The mechanics of penetration of projectiles into targets. Int J Engng Sci 1978;16:1–99.
[12] Woodward RL, Baxter BJ, Scarlett NVY. In: Harding J, editor. Mechanical properties of materials at high rates of strain. Institute of Physics Conference Series No. 70, Bristol, UK, 1984.
[13] Bai YF. Thermo-plastic instability in simple shear. J Mech Phys Solids 1982;30(4):195–207.